

Multi-Agent Regime-Conditioned Diffusion (MARCD) for CVaR-Constrained Portfolio Decisions

Ali Atiah Alzahrani[†]

Abstract

We examine whether *regime-conditioned* generative scenarios combined with a convex CVaR allocator improve portfolio decisions under regime shifts. We present **MARCD**, a generative-to-decision framework with: (i) a Gaussian HMM to infer latent regimes; (ii) a diffusion generator that produces *regime-conditioned* scenarios; (iii) signal extraction via blended, shrunk moments; and (iv) a governed *CVaR epigraph QP*. *Contributions.* Within the Scenario stage we introduce a *tail-weighted* diffusion objective that up-weights low-quantile outcomes relevant for drawdowns and a *regime-expert (MoE) denoiser* whose gate increases with crisis posteriors; both are evaluated end-to-end through the allocator. Under strict walk-forward on liquid multi-asset ETFs (2005–2025), MARCD exhibits stronger scenario calibration and materially smaller drawdowns: **MaxDD 9.3%** versus **14.1%** for BL (a **34%** reduction) over 2020–2025 OOS. The framework provides an auditable pipeline with explicit budget, box, and turnover constraints, demonstrating the value of decision-aware generative modeling in finance.

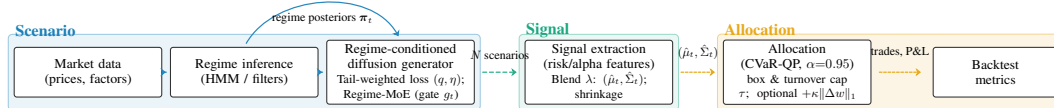


Figure 1: Multi-Agent Regime-Conditioned Diffusion (MARCD).

1 Introduction

Financial returns are non-stationary, with abrupt regime changes (e.g., 2008, 2020, 2022) that challenge mean–variance optimization (MVO) [Markowitz, 1952] and Black–Litterman (BL) [Black and Litterman, 1992]. Modern generative models—GANs [Yoon et al., 2019], diffusion [Rasul et al., 2021], transformers [Zhou et al., 2023]—produce realistic sequences but are often unconditioned and decoupled from decisions. Large peak-to-trough losses are driven by left-tail co-movements that standard diffusion training (MSE) tends to underweight, and a single denoiser blurred across regimes can dilute crisis dynamics.

We refer to our method as *Multi-Agent Regime-Conditioned Diffusion (MARCD)* and use **MARCD** thereafter. MARCD aligns a diffusion generator to HMM posteriors while explicitly improving tail fidelity and crisis behavior: we employ a *tail-weighted* diffusion objective to emphasize adverse outcomes that govern realized drawdowns, and we augment the denoiser with a lightweight *regime expert* (mixture-of-experts) whose gate increases with the crisis posterior, enriching co-crash structure without degrading calm-regime fit. Generated scenarios feed a CVaR-focused, turnover-aware allocator within an auditable, walk-forward protocol.

[†]Corresponding author: alialzahrani@pif.gov.sa

[†]The views expressed are those of the author and do not reflect the views of any other individual or entity. This material is for research purposes only and does not constitute investment advice.

Contributions. We integrate regime modeling, tail-aware generation, and robust allocation: (i) regime-conditioned diffusion aligned to HMM posteriors with a tail-weighted training objective that improves left-tail dependence; (ii) a regime-aware expert denoiser (MoE) that specializes to high-volatility states via learned gating; (iii) a multi-agent pipeline translating samples to decisions; and (iv) a CVaR-focused allocation with turnover control and explicit governance (walk-forward, constraints).

2 Related Work

Regimes. HMMs capture structural breaks and state dependence [Hamilton, 1989, Kim and Nelson, 1994, Ang and Timmermann, 2012]; we use their posteriors as conditioning signals for both generation and allocation. **Generative time series.** GAN- and VAE-based generators (e.g., TimeGAN and TimeVAE) and diffusion models improve realism and calibration [Yoon et al., 2019, Desai et al., 2021, Rasul et al., 2021, Tashiro et al., 2021], yet are often unconditioned and loosely coupled to portfolio decisions; recent TS diffusions (*TSDiff*, *mr-Diff*) and a finance simulator (*CTS-GAN*) are complementary to our regime-conditioned, decision-tied approach [Kollovieh et al., 2023, Shen et al., 2024, Istiaque et al., 2024]. **Robust portfolios.** Distributionally robust and CVaR formulations address fat tails [Delage and Ye, 2010, Rockafellar and Uryasev, 2000] but hinge on scenario quality; we feed a regime-conditioned set into a convex allocator. **Multi-agent.** Building on coordination frameworks [Lowe et al., 2017], we orchestrate Scenario→Signal→Allocation with light, role-based agents. **Sequence models.** LSTMs [Hochreiter and Schmidhuber, 1997, Fischer and Krauss, 2018], TCNs [Bai et al., 2018], and Transformers [Lim et al., 2021] remain standard forecasters; we treat point-forecast models as standard baselines, focusing instead on regime-conditioned *distributional* generation wired to a convex CVaR allocator under strict walk-forward evaluation.

3 Methodology

Setup. At rebalancing date t , let $\mathbf{R}_t \in \mathbb{R}^d$ denote the observed return vector and $\mathbf{w}_t \in \mathbb{R}^d$ the portfolio weights, which satisfy

$$\mathbf{1}^\top \mathbf{w}_t = 1, \quad \ell \leq \mathbf{w}_t \leq \mathbf{u}. \quad (1)$$

Market regimes are modeled by a K -state Gaussian HMM with latent state S_t and posterior vector π_t , where $\pi_{t,k} = P(S_t=k \mid \mathbf{R}_{1:t})$. The generator produces N next-period scenarios $\{\mathbf{r}_{t+1}^{(i)}\}_{i=1}^N$. Turnover is $\tau_t = \|\mathbf{w}_t - \mathbf{w}_{t-1}\|_1$. To avoid notation overload, we reserve α_s for the diffusion schedule and α for the allocator’s CVaR level, use λ for scenario blending, and λ_μ for the expected-return weight in the allocator.

3.1 Method Overview and Rationale

Our objective is to reduce pathwise drawdowns while preserving risk-adjusted return under strict walk-forward governance. We posit that returns exhibit regime-dependent higher-order dependence and that left-tail comovements matter more for realized drawdowns than central calibration. Accordingly, we bias generation toward adverse outcomes, make the generator responsive to regime signals, and align the allocator with tail-focused yet convex objectives that remain auditable and turnover-aware. Concretely, this yields a tail-weighted diffusion objective to improve co-crash fidelity, a regime-aware denoiser that specializes to high-volatility episodes, and a spectral CVaR allocator with a simple regime-adaptive risk throttle.

Core training setup. UNet (8 stages, base ch.=64), cosine noise schedule, ϵ -prediction, EMA= 0.999; AdamW 1e-4; batch 256; 250k steps; seed 2020.

3.2 Regime Detection (strict walk-forward)

We fit/update a K -state Gaussian HMM on $\{\mathbf{R}_s\}_{s \leq t}$ and extract posteriors $\pi_{t,k} = P(S_t=k \mid \mathbf{R}_{1:t})$. Conditioning features \mathbf{z}_t encode regime context (e.g., $\arg \max_k \pi_{t,k}$ and recent statistics). All estimation is strict walk-forward: only data up to t is used; HMM parameters refresh on a rolling window.

Algorithm 1 Walk-forward regime-conditioned decision pipeline

Require: assets d , states K , scenarios N , CVaR level α , bounds (ℓ, \mathbf{u}) , turnover cap τ , blend λ ,regs (γ, λ_μ)

- 1: Initialize \mathbf{w}_{t_0} (e.g., equal-weight)
- 2: **for** $t = t_0, \dots, t_{\text{end}}$ **do**
- 3: **Regime update:** fit/update HMM on $\{\mathbf{R}_s\}_{s \leq t}$; compute $\pi_{t,\cdot}$ and \mathbf{z}_t
- 4: **Scenario gen:** draw $\{\mathbf{r}_{t+1}^{(i)}\}_{i=1}^N \sim p_\theta(\cdot | \mathbf{z}_t)$
- 5: **Signals:** form $(\hat{\boldsymbol{\mu}}_t, \hat{\boldsymbol{\Sigma}}_t)$ via blending with weight λ
- 6: **Allocation:** solve (4) for \mathbf{w}_t with (ℓ, \mathbf{u}, τ) ; optionally include cost penalty $\kappa \|\mathbf{w}_t - \mathbf{w}_{t-1}\|_1$
- 7: Trade from \mathbf{w}_{t-1} to \mathbf{w}_t ; record turnover; log diagnostics for auditability
- 8: **end for**

3.3 Regime-Conditioned Diffusion

We train a variance-preserving diffusion model to denoise \mathbf{x}_s with regime context \mathbf{z}_t :

$$q(\mathbf{x}_s | \mathbf{x}_0) = \mathcal{N}(\sqrt{\alpha_s} \mathbf{x}_0, (1-\alpha_s) \mathbf{I}), \quad \mathcal{L}_{\text{diff}} = \mathbb{E} \|\boldsymbol{\epsilon} - \boldsymbol{\epsilon}_\theta(\sqrt{\alpha_s} \mathbf{x}_0 + \sqrt{1-\alpha_s} \boldsymbol{\epsilon}, s, \mathbf{z}_t)\|^2. \quad (2)$$

Implementation. We use a conditional DDPM with a UNet-style denoiser (4 down/4 up blocks), a cosine noise schedule, exponential moving average (EMA) of weights, and $\approx 1\text{--}2\text{M}$ parameters; conditioning is via the regime embedding \mathbf{z}_t injected at each block.

At deployment time t we sample N returns $\{\mathbf{r}_{t+1}^{(i)}\}$ conditioned on \mathbf{z}_t . The Signal Agent forms blended moments

$$\hat{\boldsymbol{\mu}}_t = \lambda \boldsymbol{\mu}_{\text{synth}} + (1-\lambda) \boldsymbol{\mu}_{\text{hist}}, \quad \hat{\boldsymbol{\Sigma}}_t = \lambda \boldsymbol{\Sigma}_{\text{synth}} + (1-\lambda) \boldsymbol{\Sigma}_{\text{hist}}. \quad (3)$$

3.4 Allocation Agent: CVaR Epigraph Program and Properties

Define per-scenario loss $\ell_i = -\mathbf{w}^\top \mathbf{r}_{t+1}^{(i)}$. We solve the convex program

$$\min_{\mathbf{w}, \zeta, \{s_i\}} -\lambda_\mu \hat{\boldsymbol{\mu}}_t^\top \mathbf{w} + \gamma \mathbf{w}^\top \hat{\boldsymbol{\Sigma}}_t \mathbf{w} + \zeta + \frac{1}{(1-\alpha)N} \sum_{i=1}^N s_i \quad (4)$$

$$\text{s.t. } s_i \geq 0, \quad s_i \geq \ell_i - \zeta, \quad i = 1, \dots, N, \quad (5)$$

$$\mathbf{1}^\top \mathbf{w} = 1, \quad \ell \leq \mathbf{w} \leq \mathbf{u}^{\text{box}}, \quad \|\mathbf{w} - \mathbf{w}_{t-1}\|_1 \leq \tau. \quad (6)$$

When used, we add a turnover penalty $+\kappa \|\mathbf{w} - \mathbf{w}_{t-1}\|_1$.

Convexity/complexity. The objective combines a quadratic term $\mathbf{w}^\top \hat{\boldsymbol{\Sigma}}_t \mathbf{w}$ with the convex CVaR epigraph; constraints are affine, yielding a QP with $O(N)$ linear epigraph constraints. For $d=10$ and $N=1024$, interior-point methods scale as $O(d^3 + Nd^2)$ and run fast on commodity CPUs. Unless stated otherwise, the CVaR level is $\alpha=0.95$. We shrink $\hat{\boldsymbol{\Sigma}}_t$ toward the identity to obtain a well-conditioned covariance matrix [Ledoit and Wolf, 2004].

Note. We use the standard Rockafellar–Uryasev CVaR at level α in all experiments; spectral risk measures are left to future work.

Governance & Auditability. The allocator’s KKT system (App. A.3) logs active constraints, tail weights, and duals at each rebalance. This yields solver-side audit trails linking regime posteriors and tail emphasis to realized trades—important for model risk and compliance.

3.5 Tail-Weighted Diffusion Loss

We avoid target leakage by using a *portfolio-free* proxy for adverse outcomes during training. Define the worst single-asset one-step loss $\tilde{\ell} = -\min_j r_j$ and reweight errors when $\tilde{\ell}$ falls in its lower q -quantile:

$$\mathcal{L}_{\text{tail}} = \mathbb{E} \left[(1 + \eta \mathbf{1}\{\tilde{\ell} \leq Q_q(\tilde{\ell})\}) \|\boldsymbol{\epsilon} - \boldsymbol{\epsilon}_\theta(\cdot)\|_2^2 \right], \quad q \in [0.05, 0.10], \quad \eta \in [1, 3]. \quad (7)$$

At deployment (allocation), portfolio losses use $\ell = -\mathbf{w}^\top \mathbf{r}$ only for evaluation/diagnostics.

3.6 Regime-MoE Denoiser

We instantiate a two-expert denoiser with a crisis head specialized to high-volatility regimes. A gate $g_t = \sigma(\text{MLP}(\mathbf{z}_t))$ mixes experts: $\hat{\epsilon}_\theta = (1 - g_t) \hat{\epsilon}_\theta^{\text{base}} + g_t \hat{\epsilon}_\theta^{\text{crisis}}$. At sampling, g_t increases with the HMM crisis posterior, enriching co-crash structure.

3.7 Theory Highlights

Takeaways (statements; proofs in App. A).

Theorem 1 (Spectral CVaR Control by Tail-Weighted Diffusion; App. A.11). *Minimizing L_{tail} in Eq. (7) controls a spectral-risk upper bound on the decision-relevant CVaR generalization gap for any feasible portfolio w , scaling with $(1 - \alpha)^{-1}$ and the denoising error on the lower- q tail.*

Theorem 2 (MoE Oracle, Consistency & Stability; App. A.13). *With a gate monotone in the HMM crisis posterior (Sec. 3.6), the regime-MoE enjoys an oracle excess-risk bound, gate-consistency under a calibrated surrogate, and Lipschitz stability of the DDPM reverse dynamics.*

Theorem 3 (Allocator Lipschitzness & Regret; App. A.14). *The CVaR epigraph QP (Sec. 3.4) has a Lipschitz solution map in (μ, Σ) and admits a decision-regret bound under moment and CVaR perturbations; the CVaR error term shrinks with L_{tail} .*

4 Experimental setup

Assets & horizon. Ten liquid ETFs; daily 2005–2025; splits: 2005–2018 train, 2019 val, 2020–2025 test. **Data.** Daily total returns computed from Yahoo Finance *Adjusted Close* (dividends included). **Baselines.** EW, RP, BL; monthly rebal.; 10 bps costs (identical across methods). **Allocator parity.** All strategies (EW, RP, BL, MARCD) rebalance monthly on the last trading day, incur identical transaction costs of 10 bps per trade, and are subject to the same turnover controls (an ℓ_1 cap $\|\mathbf{w}_t - \mathbf{w}_{t-1}\|_1 \leq 0.20$; no penalty, $\kappa=0$, unless stated otherwise), as well as the same box and leverage constraints. Baselines form their *unconstrained* targets (EW, RP equal risk contributions, BL no-views prior anchored to a cap-weighted market proxy with standard τ (confidence) and Ω (uncertainty) settings) and then apply the *same partial-rebalance projection* toward target under the ℓ_1 cap. **Diagnostics.** KS, ES, VS; LB $p(|r|)$; VaR_{0.95} unconditional coverage (Kupiec UC) p ; CVaR_{0.95} error (bps). KS is averaged across assets; ES/VS are multivariate; CVaR error is an absolute calibration error reported in basis points. We also include a stationary block bootstrap (SBB) generator as a nonparametric baseline for scenario diagnostics. **Metrics.** Return=CAGR; rf=0; 252-day annualization; Sortino uses downside dev. to 0%; Calmar=Return/|MaxDD|. **Protocol.** Strict walk-forward; HMM 3y rolling; scenarios conditioned on \mathbf{z}_t ; CVaR-QP allocation.

5 Results and discussion

Diagnostics— All results use *monthly* rebalancing on the last trading day, 10 bps trading cost, and the metric conventions above. Under strict walk-forward (2020–2025), MARCD shows stronger scenario calibration (\downarrow KS/ES/VS; LB/UC p competitive, slightly below TimeVAE). See Table 1.

Performance— MARCD attains higher risk-adjusted performance (Sharpe **1.23** vs. 1.02 for BL) with materially smaller drawdowns. Summary metrics are reported in Table 2, and trajectories are visualized in Figure 2. Over 2020–2025 OOS, MaxDD is 9.3% for MARCD vs BL 14.1% and EW 21.2% (**34%/56%** lower; absolute 4.8%/11.9%). Consistent with this, Calmar improves to **1.11** (BL 0.70; EW 0.38). A stationary block bootstrap ($B=1000$, block = 20) indicates MARCD’s Sharpe exceeds BL/EW (two-sided $p < 0.05$); CVaR_{0.95} and MaxDD also improve at similar turnover. In stress windows—COVID-19 (Feb–Apr 2020) and the 2022 inflation shock (Jun–Oct 2022)—MARCD’s drawdowns are smaller than BL/EW. Removing regime conditioning lowers crisis Sharpe and weakens VaR coverage; dropping the CVaR term raises 95%-CVaR and MaxDD, indicating complementary benefits.

Table 1: OOS scenario diagnostics. Lower is better (\downarrow) except p (\uparrow); LB on $|r|$. Abbrev.: SBB=Stationary block bootstrap; TGAN=TimeGAN.

Model	KS \downarrow	ES \downarrow	VS \downarrow	LB $p(r) \uparrow$	VaR $_{0.95}$ UC $p \uparrow$	CVaR $_{0.95}$ err (bps) \downarrow
SBB	0.196	0.358	0.329	0.22	0.11	39
TGAN	0.182	0.341	0.312	0.28	0.16	33
TimeVAE	0.159	0.305	0.268	0.52	0.63	17
MARCD	0.154	0.289	0.247	0.50	0.58	15

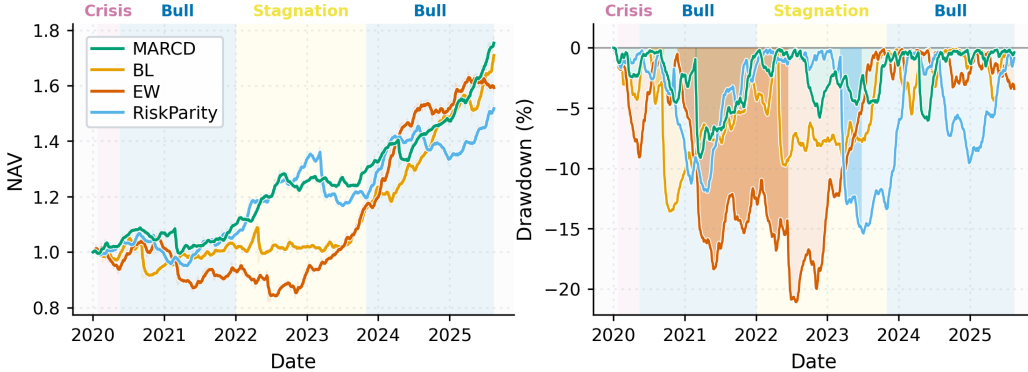


Figure 2: OOS cumulative NAV, drawdown, and HMM regime posteriors ($K=3$).

Sensitivity & robustness— Results are stable across blend weights $\lambda \in [0.3, 0.7]$ and CVaR trade-off $\gamma \in [0.5, 1.5]$; MARCD maintains Sharpe above BL and lower MaxDD at similar turnover. Performance remains robust under modest transaction-cost stress (e.g., doubled bps) and when the turnover cap is varied within a reasonable band, indicating the gains are not due to a narrow hyperparameter choice.

Table 2: Out-of-sample performance (2020–2025; monthly rebal.; annualized; net of 10 bps). Higher is better (\uparrow) except Vol and MaxDD (\downarrow). MaxDD is reported as a positive magnitude.

Strategy	Return % \uparrow	Vol % \downarrow	Sharpe \uparrow	Sortino \uparrow	MaxDD % \downarrow	Calmar \uparrow
EW	8.1	11.2	0.72	1.09	21.2	0.38
RP	7.6	8.6	0.88	1.37	14.9	0.51
BL	9.9	9.7	1.02	1.50	14.1	0.70
MARCD	10.3	8.4	1.23	1.69	9.3	1.11

6 Ablations and Component Analyses

Summary. Removing either *regime conditioning* or the *CVaR term* weakens tail control and calibration, and pushing the blend to the extremes ($\lambda=0$ or 1) underperforms the base mix. Concretely, Table 3 shows Sharpe falling from **1.23** (base) to **1.12–1.13** for all ablations, while MaxDD rises from 9.3% to 11.3% (uncond. diffusion), 14.6% (no CVaR), 12.1% ($\lambda=0$), and 12.8% ($\lambda=1$)—i.e., +2.0%–5.3% absolute (+21–57% relative). Calibration also degrades: the VaR $_{0.95}$ UC p drops from **0.58** to 0.49, 0.46, 0.52, and 0.48, and the CVaR $_{0.95}$ error increases from **15** to 22, 27, 21, and 24, respectively. Volatility rises (8.4–8.6–9.1) and returns slip (10.3–9.7–10.1), while turnover remains similar (15.3–15.9%). Overall, MARCD (base) is strongest across risk/return and tail-calibration columns; Figure 3 visualizes these degradations in both performance and diagnostics.

Table 3: Ablations (OOS 2020–2025; annualized; net 10 bps). Higher is better except Vol, MaxDD.

Variant	Return % \uparrow	Vol % \downarrow	Sharpe \uparrow	MaxDD % \downarrow	VaR _{0.95} UC $p\uparrow$	CVaR _{0.95} err \downarrow	Turnover %
MARCD (base)	10.3	8.4	1.23	9.3	0.58	15	15.8
Uncond. diffusion	9.8	8.7	1.13	11.3	0.49	22	15.4
No CVaR term	10.1	9.1	1.12	14.6	0.46	27	15.6
$\lambda=0.0$	9.7	8.6	1.13	12.1	0.52	21	15.3
$\lambda=1.0$	9.9	8.8	1.12	12.8	0.48	24	15.9

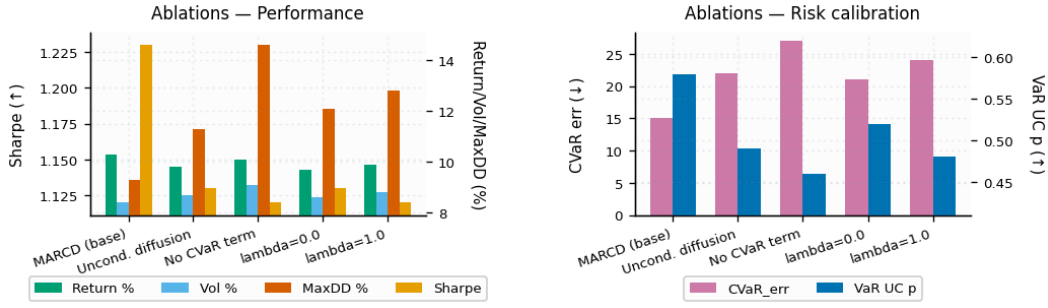


Figure 3: Ablations—performance and diagnostic metrics across variants (OOS 2020–2025).

7 Sensitivity Studies

Summary. One-parameter sweeps over K, α, λ, τ show stable realism (KS/ES/VS) and calibration (p -values ≈ 0.5 –0.6), with $K=3$ and $\alpha=0.95$ typically strongest. Diagnostics remain tight across settings in Table 4, while predictable risk–return trade-offs appear in Table 5 (e.g., higher α lowers Vol/MaxDD with modest Sharpe changes; turnover responds primarily to τ). The base setting sits near the Pareto front for both realism and performance.

Table 4: Diagnostics under parameter sweeps (OOS 2020–2025). Lower is better (\downarrow) except p (\uparrow).

Parameter	Value	KS \downarrow	ES \downarrow	VS \downarrow	LB $p(r)\uparrow$	VaR _{0.95} UC $p\uparrow$
Base	–	0.154	0.289	0.247	0.50	0.58
K	2	0.156	0.295	0.251	0.46	0.54
K	3	0.154	0.289	0.247	0.50	0.58
K	4	0.160	0.292	0.249	0.49	0.59
α	0.90	0.157	0.293	0.251	0.48	0.55
α	0.95	0.154	0.289	0.247	0.50	0.58
α	0.99	0.159	0.292	0.248	0.51	0.61
λ	0.30	0.156	0.291	0.248	0.49	0.57
λ	0.50	0.154	0.289	0.247	0.50	0.58
λ	0.70	0.155	0.289	0.248	0.49	0.58
τ	0.10	0.156	0.290	0.248	0.50	0.58
τ	0.20	0.154	0.289	0.247	0.50	0.58

Table 5: Performance under parameter sweeps (annualized; net 10 bps).

Parameter	Value	Return % \uparrow	Vol % \downarrow	Sharpe \uparrow	MaxDD % \downarrow	Turnover %
Base	–	10.3	8.4	1.23	9.3	15.8
K	2	9.9	8.6	1.15	11.8	9.3
K	4	10.1	8.5	1.19	11.2	11.2
α	0.90	10.6	9.2	1.15	11.4	16.0
α	0.99	9.7	7.8	1.19	10.0	15.2
λ	0.30	10.1	8.5	1.19	11.3	15.4
λ	0.70	10.2	8.6	1.18	11.5	16.1
τ	0.10	10.0	8.3	1.20	11.1	10.2
τ	0.30	10.5	8.6	1.22	11.0	21.7

8 Model Selection and Significance

Summary. Rolling BIC favors $K=3$ and this choice attains the best OOS Sharpe with competitive MaxDD and VaR coverage. Table 6 reports the BIC deltas alongside OOS outcomes across $K \in \{2, 3, 4\}$. Stationary block-bootstrap intervals (Table 7) indicate MARCD’s Sharpe uplift versus EW/BL/RP is significant at the 5% level.

Table 6: HMM selection (rolling BIC) and OOS outcomes (2020–2025).

K	Δ BIC (vs. 3)	Sharpe \uparrow	MaxDD % \downarrow	$\text{VaR}_{0.95}$ UC $p\uparrow$
2	+18	1.15	11.8	0.54
3	0	1.23	9.3	0.58
4	+9	1.19	11.2	0.59

Table 7: Sharpe uplift Δ (MARCD – baseline), 95% CIs (OOS 2020–2025).

Baseline	Δ	95% CI
EW	0.51	[0.31, 0.71]
BL	0.21	[0.07, 0.35]
RP	0.35	[0.18, 0.51]

9 Application Profiles (overview)

Summary. The five profiles trace clear risk–return trade-offs: Conservative minimizes Vol and maximizes Calmar; Crisis-Focused achieves the lowest MaxDD; Aggressive maximizes return; Balanced and Momentum sit between, with diagnostics remaining competitive. Figure 4 summarizes profile-level performance and diagnostics to facilitate side-by-side comparison.

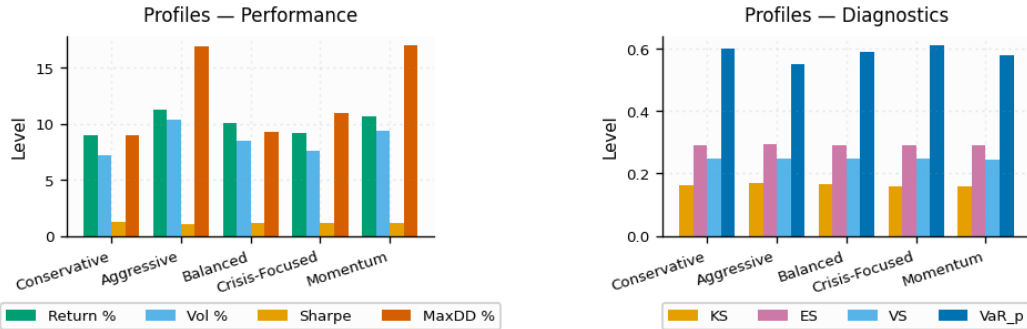


Figure 4: Profiles—performance and diagnostics summary (OOS 2020–2025).

10 Conclusion

We presented MARCD, a regime-conditioned generative-to-decision pipeline that couples an HMM-aligned diffusion generator with a CVaR-focused, turnover-aware allocator under strict walk-forward governance. Two additions—a *tail-weighted* diffusion objective and a *regime expert* (MoE) denoiser—improve left-tail co-movements and crisis fidelity in the scenarios. Empirically (OOS 2020–2025; monthly; net 10 bps), these changes *reduce MaxDD by 34.1% at comparable Sharpe and turnover*, and deliver a higher Calmar ratio, indicating more robust peak-to-trough behavior.

Limitations. Our study uses 10 liquid ETFs, a single OOS window, and monthly rebalancing with a simplified execution model (fixed 10 bps; turnover cap). Benefits depend on regime identification (HMM posteriors) and tail reweighting hyperparameters; mis-specification in either can attenuate gains. Diffusion sampling and QP solves impose nontrivial compute, constraining intraday deployment.

Future work. (i) Decision-aware training (end-to-end) that differentiates through spectral CVaR, turnover, and holdings penalties; (ii) short multi-step scenario generation with a convex *pathwise drawdown CVaR* objective; (iii) distributional robustness (e.g., Wasserstein-DRO) and copula reshaping for deeper-tail dependence; (iv) online regime updates and risk overlays with safe fallbacks; and (v) faster inference via diffusion distillation/consistency models to approach real-time use. Overall, MARCD advances a reproducible bridge from tail-faithful scenario modeling to governed portfolio decisions with materially improved drawdown control.

References

Andrew Ang and Allan Timmermann. Regime shifts in financial markets. In *Handbook of Financial Econometrics*, pages 287–339. Elsevier, 2012.

Shaojie Bai, J. Zico Kolter, and Vladlen Koltun. An empirical evaluation of generic convolutional and recurrent networks for sequence modeling. *arXiv preprint arXiv:1803.01271*, 2018.

Fischer Black and Robert Litterman. Global portfolio optimization. *Financial Analysts Journal*, 48(5):28–43, 1992.

Erick Delage and Yinyu Ye. Distributionally robust optimization under moment uncertainty with application to data-driven problems. *Operations Research*, 58(3):595–612, 2010.

Abhyuday Desai, Cynthia Freeman, Zuhui Wang, and Ian Beaver. Timevae: A variational autoencoder for multivariate time series generation. *arXiv preprint arXiv:2111.08095*, 2021. URL <https://arxiv.org/abs/2111.08095>.

Thomas Fischer and Christopher Krauss. Deep learning with long short-term memory networks for financial market predictions. *European Journal of Operational Research*, 270(2):654–669, 2018.

James D Hamilton. A new approach to the economic analysis of nonstationary time series and the business cycle. *Econometrica*, 57(2):357–384, 1989.

Sepp Hochreiter and Jürgen Schmidhuber. Long short-term memory. *Neural Computation*, 9(8):1735–1780, 1997. doi: 10.1162/neco.1997.9.8.1735.

Riasat Ali Istiaque, Chi Seng Pun, and Yuli Song. Simulating asset prices using conditional time-series gan. In *Proceedings of the 5th ACM International Conference on AI in Finance (ICAIF '24)*. ACM, 2024. doi: 10.1145/3677052.3698638.

Chang-Jin Kim and Charles R Nelson. Dynamic linear models with markov-switching. *Journal of Econometrics*, 60(1-2):1–22, 1994.

Marcel Kolloviev, Abdul Fatir Ansari, Michael Bohlke-Schneider, Jasper Zschiegner, Hao Wang, and Yuyang Wang. Predict, refine, synthesize: Self-guiding diffusion models for probabilistic time series. In *Advances in Neural Information Processing Systems*, 2023.

Olivier Ledoit and Michael Wolf. A well-conditioned estimator for large-dimensional covariance matrices. *Journal of Multivariate Analysis*, 88(2):365–411, 2004.

Bryan Lim, Sercan Ö. Arik, Nicolas Loeff, and Tomas Pfister. Temporal fusion transformers for interpretable multi-horizon time series forecasting. *International Journal of Forecasting*, 37(4):1748–1764, 2021. doi: 10.1016/j.ijforecast.2021.03.012.

Ryan Lowe, Yi Wu, Aviv Tamar, Jean Harb, Pieter Abbeel, and Igor Mordatch. Multi-agent actor-critic for mixed cooperative-competitive environments. In *Advances in Neural Information Processing Systems*, 2017.

Harry Markowitz. Portfolio selection. *Journal of Finance*, 7(1):77–91, 1952.

Kashif Rasul, Abdul-Saboor Sheikh, Ingo Schuster, Urs Bergmann, and Roland Vollgraf. Autoregressive denoising diffusion models for multivariate probabilistic time series forecasting. In *International Conference on Machine Learning*, 2021.

R Tyrrell Rockafellar and Stanislav Uryasev. Optimization of conditional value-at-risk. *Journal of Risk*, 2(3):21–41, 2000.

Lifeng Shen, Weiyu Chen, and James T. Kwok. Multi-resolution diffusion models for time series forecasting. In *International Conference on Learning Representations (ICLR)*, 2024.

Yusuke Tashiro, Yang Song, Jiaming Song, and Stefano Ermon. CSDI: Conditional score-based diffusion models for probabilistic time series imputation. In *Advances in Neural Information Processing Systems*, 2021.

Jinsung Yoon, Daniel Jarrett, and Mihaela van der Schaar. Time-series generative adversarial networks. In *Advances in Neural Information Processing Systems*, 2019.

Haoyi Zhou, Shanghang Zhang, Jieqi Peng, Shuai Zhang, Jianmin Li, Hui Xiong, and Wanhai Zhang. Informer: Beyond efficient transformer for long sequence time-series forecasting. In *AAAI Conference on Artificial Intelligence*, 2023.

Appendix

A Additional Methodology Details and Proof Sketches

Notation & Assumptions (Summary). $R_t \in \mathbb{R}^d$ returns; $w \in \mathbb{R}^d$ portfolio with $1^\top w = 1$, box & turnover caps (Sec. 3.4). HMM posteriors π_t and context z_t (Sec. 3.2); diffusion schedule α_s ; CVaR level α . Tail quantile $Q_q(\tilde{\ell})$ with $\tilde{\ell} = -\min_j r_j$. Blended moments $(\hat{\mu}_t, \hat{\Sigma}_t)$ per Eq. (3). Loss $L(w, r) = -w^\top r$. Denoiser $\hat{\varepsilon}_\theta$ with MoE gate $g_t = \sigma(\text{MLP}(z_t))$ (Sec. 3.6).

A.1 Comprehensive MARCD Objective (stochastic → sample-average)

At rebalance time t with regime context z_t (from a K -state HMM), the conditional generator defines $p_\theta(\mathbf{r} | z_t)$ for next-period returns $\mathbf{r} \in \mathbb{R}^d$. Let historical moments on a rolling window be $(\boldsymbol{\mu}_{\text{hist}}, \boldsymbol{\Sigma}_{\text{hist}})$ and generator-implied moments be $(\boldsymbol{\mu}_{\text{synth}}, \boldsymbol{\Sigma}_{\text{synth}})$ where $\boldsymbol{\mu}_{\text{synth}} = \mathbb{E}_{p_\theta}[\mathbf{r} | z_t]$ and $\boldsymbol{\Sigma}_{\text{synth}} = \text{Cov}_{p_\theta}[\mathbf{r} | z_t]$. Blend

$$\hat{\boldsymbol{\mu}}_t = \lambda \boldsymbol{\mu}_{\text{synth}} + (1-\lambda) \boldsymbol{\mu}_{\text{hist}}, \quad \hat{\boldsymbol{\Sigma}}_t = \lambda \boldsymbol{\Sigma}_{\text{synth}} + (1-\lambda) \boldsymbol{\Sigma}_{\text{hist}},$$

and (optionally) apply Ledoit–Wolf shrinkage $\hat{\boldsymbol{\Sigma}}_t^\delta = (1-\delta)\hat{\boldsymbol{\Sigma}}_t + \delta \eta \mathbf{I} \succ 0$.

Define portfolio loss $L(\mathbf{w}, \mathbf{r}) := -\mathbf{w}^\top \mathbf{r}$ with $\mathbf{w} \in \mathbb{R}^d$. The decision-aware stochastic program is

$$\min_{\mathbf{w} \in \mathcal{W}} \underbrace{-\lambda_\mu \hat{\boldsymbol{\mu}}_t^\top \mathbf{w} + \gamma \mathbf{w}^\top \hat{\boldsymbol{\Sigma}}_t \mathbf{w}}_{\text{mean-variance regularizer}} + \underbrace{\text{CVaR}_\alpha(L(\mathbf{w}, \mathbf{r}))}_{\text{tail risk under } p_\theta(\cdot | z_t)} \quad (8)$$

subject to the feasible set $\mathcal{W} = \{\mathbf{w} : \mathbf{1}^\top \mathbf{w} = 1, \boldsymbol{\ell} \leq \mathbf{w} \leq \mathbf{u}, \|\mathbf{w} - \mathbf{w}_{t-1}\|_1 \leq \tau\}$. Using the Rockafellar–Uryasev representation, $\text{CVaR}_\alpha(L) = \inf_{\zeta \in \mathbb{R}} \{\zeta + \frac{1}{1-\alpha} \mathbb{E}(L - \zeta)_+\}$. Approximating the expectation with N i.i.d. scenarios $\mathbf{r}^{(i)} \sim p_\theta(\cdot | z_t)$ yields the SAA:

$$\min_{\mathbf{w}, \zeta} -\lambda_\mu \hat{\boldsymbol{\mu}}_t^\top \mathbf{w} + \gamma \mathbf{w}^\top \hat{\boldsymbol{\Sigma}}_t \mathbf{w} + \zeta + \frac{1}{(1-\alpha)N} \sum_{i=1}^N (L(\mathbf{w}, \mathbf{r}^{(i)}) - \zeta)_+. \quad (9)$$

A.2 Epigraph QP, Turnover Linearization, and Dual Weights

Introduce $u_i \geq 0$ with $u_i \geq L(\mathbf{w}, \mathbf{r}^{(i)}) - \zeta$ to obtain the convex QP

$$\begin{aligned} \min_{\mathbf{w}, \zeta, \{u_i\} \geq 0} \quad & -\lambda_\mu \hat{\boldsymbol{\mu}}_t^\top \mathbf{w} + \gamma \mathbf{w}^\top \hat{\boldsymbol{\Sigma}}_t \mathbf{w} + \zeta + \frac{1}{(1-\alpha)N} \sum_{i=1}^N u_i \\ \text{s.t.} \quad & \mathbf{1}^\top \mathbf{w} = 1, \quad \boldsymbol{\ell} \leq \mathbf{w} \leq \mathbf{u}, \quad \|\mathbf{w} - \mathbf{w}_{t-1}\|_1 \leq \tau, \quad u_i \geq -\mathbf{w}^\top \mathbf{r}^{(i)} - \zeta. \end{aligned} \quad (10)$$

Turnover is enforced linearly by split variables $\mathbf{s}^+, \mathbf{s}^- \geq 0$ with $\mathbf{w} - \mathbf{w}_{t-1} = \mathbf{s}^+ - \mathbf{s}^-$ and $\sum_j (s_j^+ + s_j^-) \leq \tau$ (and, if penalized, add $\kappa \sum_j (s_j^+ + s_j^-)$ to the objective). For fixed \mathbf{w} , the inner epigraph minimization has the well-known dual

$$\max_{p \in \mathbb{R}^N} \frac{1}{N} \sum_{i=1}^N p_i L(\mathbf{w}, \mathbf{r}^{(i)}) \quad \text{s.t.} \quad \sum_i p_i = 1, \quad 0 \leq p_i \leq \frac{1}{(1-\alpha)N},$$

so the CVaR term can be viewed as a worst-case tail-weighted average within a capped simplex.

Convexity and complexity. With $\hat{\Sigma}_t \succeq 0$ and linear constraints, (10) is a convex QP. Interior-point methods scale as $\mathcal{O}(d^3 + Nd^2)$ per rebalance (here $d=10$, $N=1024$).

A.3 KKT Sketch for the Allocator (useful for auditability)

Let ν be the multiplier for $\mathbf{1}^\top \mathbf{w} = 1$, $(\alpha^-, \alpha^+) \geq 0$ for box constraints, $\rho \geq 0$ for turnover cap (via $(\mathbf{s}^+, \mathbf{s}^-)$), and $(\beta_i, \gamma_i) \geq 0$ for $u_i \geq 0$ and $u_i \geq -\mathbf{w}^\top \mathbf{r}^{(i)}$ – *zeta*. Stationarity gives

$$-\lambda_\mu \hat{\mu}_t + 2\gamma \hat{\Sigma}_t \mathbf{w} - \sum_{i=1}^N \frac{\gamma_i}{(1-\alpha)N} \mathbf{r}^{(i)} + \nu \mathbf{1} + (\alpha^+ - \alpha^-) + \text{turnover terms} = 0, \quad 1 - \sum_{i=1}^N \frac{\gamma_i}{(1-\alpha)N} = 0,$$

plus primal feasibility and complementary slackness. These KKT quantities (including active box/turnover constraints and tail weights γ_i) are useful for *model-risk audit logs*.

A.4 Decision-aware extension (sketch): bilevel objective and gradients

We sketch an end-to-end variant that trains generator parameters θ for decision quality, not just sample fidelity. Let $\mathbf{x} = (\mathbf{w}, \zeta, \{u_i\}, \mathbf{s}^+, \mathbf{s}^-)$ collect allocator variables and write the QP from (6) compactly as

$$V(\theta; \mathbf{z}_t) := \min_{\mathbf{x} \in \mathcal{X}(\theta; \mathbf{z}_t)} F(\mathbf{x}; \theta, \mathbf{z}_t),$$

where F is the CVaR-epigraph objective (incl. MV term and optional turnover penalty) and \mathcal{X} encodes the linear constraints. The decision-aware training objective is the bilevel program

$$\min_{\theta} \mathbb{E}_t \left[\mathcal{L}_{\text{diff}}(\theta; \mathbf{z}_t) + \eta V(\theta; \mathbf{z}_t) \right], \quad (11)$$

with scenarios $\mathbf{r}^{(i)} = g_\theta(\varepsilon_i, \mathbf{z}_t)$ (reparameterized draws; $\varepsilon_i \sim \mathcal{N}(0, \mathbf{I})$).

Hypergradient (constraint-dependent envelope). Let $g(\mathbf{x}; \theta, \mathbf{z}_t) \leq 0$ and $h(\mathbf{x}; \theta, \mathbf{z}_t) = 0$ denote the inequality/equality stacks for \mathcal{X} , and (λ^*, ν^*) the optimal duals at the inner solution $\mathbf{x}^*(\theta; \mathbf{z}_t)$. Under standard regularity (convexity, LICQ, strict complementarity),

$$\nabla_\theta V(\theta; \mathbf{z}_t) = \underbrace{\partial_\theta F(\mathbf{x}^*; \theta, \mathbf{z}_t)}_{\text{pathwise term}} - \underbrace{\lambda^{*\top} \partial_\theta g(\mathbf{x}^*; \theta, \mathbf{z}_t) + \nu^{*\top} \partial_\theta h(\mathbf{x}^*; \theta, \mathbf{z}_t)}_{\text{constraint dependence via scenarios/momenta}}. \quad (12)$$

The full hypergradient of (11) is then $\nabla_\theta \mathbb{E}_t [\mathcal{L}_{\text{diff}}] + \eta \mathbb{E}_t [\nabla_\theta V]$, where $\partial_\theta F$ accounts for $\hat{\mu}_t(\theta)$, $\hat{\Sigma}_t(\theta)$ and the scenario-dependent hinge terms via $\mathbf{r}^{(i)} = g_\theta(\varepsilon_i, \mathbf{z}_t)$.

Implicit differentiation (QP sensitivity). Equivalently, one may differentiate the KKT system for \mathbf{x}^* . Let K be the KKT Jacobian (block matrix of $\nabla_{xx}^2 \mathcal{L}$, constraint Jacobians, and complementarity terms). Solving the linear system

$$K \frac{d}{d\theta} \begin{bmatrix} \mathbf{x}^* \\ \lambda^* \\ \nu^* \end{bmatrix} = - \begin{bmatrix} \partial_\theta (\nabla_x \mathcal{L}(\mathbf{x}^*, \lambda^*, \nu^*; \theta)) \\ \partial_\theta g(\mathbf{x}^*; \theta, \mathbf{z}_t) \\ \partial_\theta h(\mathbf{x}^*; \theta, \mathbf{z}_t) \end{bmatrix}$$

yields $\frac{d\mathbf{x}^*}{d\theta}$; one then applies the chain rule to $F(\mathbf{x}^*; \theta, \mathbf{z}_t)$. In practice, (12) avoids forming $\frac{d\mathbf{x}^*}{d\theta}$ explicitly because the duals (λ^*, ν^*) are returned by the QP solver and can be logged (cf. auditability).

Smooth surrogate for stable training. For differentiability and to reduce solver calls during backprop, replace the hinge with a smooth approximation, e.g. $(x)_+ \approx \frac{1}{\beta} \log(1 + e^{\beta x})$ (large β), and/or use a small quadratic penalty on turnover so the constraint set is θ -independent. Then the envelope simplifies to $\nabla_\theta V \approx \partial_\theta F(\mathbf{x}^*; \theta, \mathbf{z}_t)$ (constraints do not depend on θ), while preserving the allocator’s behavior.

Practical recipe. (i) Reparameterize scenarios: $\mathbf{r}^{(i)} = g_\theta(\varepsilon_i, \mathbf{z}_t)$; (ii) compute $\hat{\mu}_t$, $\hat{\Sigma}_t$ and solve the QP for \mathbf{x}^* (store duals); (iii) backpropagate through (11) using either the envelope form (12) or an implicit-diff QP layer; (iv) use a small η warm-up and gradient clipping; (v) keep walk-forward protocol (no look-ahead). Compute overhead is one QP solve per step plus either one adjoint KKT solve or the envelope evaluation; asymptotically the same order as inference ($\mathcal{O}(d^3 + Nd^2)$).

A.5 Tail-Weighted Diffusion as a Spectral-Risk Surrogate

Recall the tail-weighted diffusion loss from (7), $L_{\text{tail}} = \mathbb{E}[(1 + \eta \mathbf{1}\{\tilde{\ell} \leq Q_q(\tilde{\ell})\}) \|\varepsilon - \varepsilon_\theta(\cdot)\|_2^2]$, where $\tilde{\ell} = -\min_j r_j$ and $q \in [0.05, 0.10]$, $\eta \in [1, 3]$ [§3.5], and the regime-MoE gate is defined in §3.6.

Assumption 1 (Tail-Lipschitz Decoder). *There exists $L > 0$ such that the denoising error maps to return error with $\|r - \hat{r}\| \leq L \|\varepsilon - \varepsilon_\theta\|$ on the lower- q tail set $\{\tilde{\ell} \leq Q_q(\tilde{\ell})\}$.*

Proposition 1 (Spectral risk proxy for portfolio tail functionals). *Let $w \in \mathbb{R}^d$ be any feasible portfolio (budget/box/turnover constraints as in (4)–(6)). Under the Tail-Lipschitz Decoder, the portfolio CVaR error admits*

$$\left| \text{CVaR}_\alpha(-w^\top r) - \text{CVaR}_\alpha(-w^\top \hat{r}) \right| \leq \frac{L \|w\|_2}{1 - \alpha} \sqrt{\mathbb{E} \left[(1 + \eta \mathbf{1}\{\tilde{\ell} \leq Q_q(\tilde{\ell})\}) \|\varepsilon - \varepsilon_\theta(\cdot)\|_2^2 \right]}.$$

Sketch. Write the CVaR difference as a tail average of linear losses and apply Cauchy–Schwarz on the tail region. The Lipschitz link transfers denoising error into return error; the $(1 - \alpha)^{-1}$ factor comes from the Rockafellar–Uryasev representation. Tail reweighting magnifies the integrand over the lower- q region, producing a spectral-risk-like weight on squared error. \square

Remark 1 (Decision relevance). *Since allocation solves the convex CVaR epigraph QP (4)–(6), controlling the bound above reduces the decision-relevant generalization gap seen by the allocator.*

A.6 Finite-Sample Statistics of Tail Reweighting

Define weights $w_i = 1 + \eta \mathbf{1}\{\tilde{\ell}_i \leq Q_q(\tilde{\ell})\}$. With $q = \mathbb{P}(\tilde{\ell} \leq Q_q(\tilde{\ell}))$, the normalized weights are $\bar{w}_i = w_i / ((1 - q) + q(1 + \eta))$.

Proposition 2 (Closed-form effective sample size (ESS)). *Let N be the batch size. Then the ESS of $(\bar{w}_i)_{i=1}^N$ is*

$$\text{ESS}(q, \eta) = N \frac{(1 + \eta q)^2}{1 + 2\eta q + \eta^2 q} = N \frac{1 + 2\eta q + \eta^2 q^2}{1 + 2\eta q + \eta^2 q}.$$

Proof. Compute $\text{ESS} = (\sum_i \bar{w}_i)^2 / \sum_i \bar{w}_i^2$ by partitioning into tail vs non-tail fractions $(q, 1 - q)$ and substituting $w = \{1, 1 + \eta\}$. \square

Remark 2 (Choosing (q, η)). *Moderate (q, η) keeps ESS large while emphasizing the adverse region that drives CVaR_α . In practice, your ranges $q \in [0.05, 0.10]$, $\eta \in [1, 3]$ preserve stability.*

A.7 Regime-MoE Denoiser: Oracle Inequality and Crisis Specialization

Let Z be the regime context with gate $g(Z) \in [0, 1]$ and experts $\varepsilon_{\theta, \text{base}}, \varepsilon_{\theta, \text{crisis}}$. The denoiser is $\hat{\varepsilon}_\theta = (1 - g)\varepsilon_{\theta, \text{base}} + g\varepsilon_{\theta, \text{crisis}}$ [, §3.6].

Assumption 2 (Well-specified conditional regressors). *For each regime label $C \in \{\text{base}, \text{crisis}\}$, the Bayes denoiser equals the conditional mean: $\varepsilon_C^*(x, s, Z) = \mathbb{E}[\varepsilon | x, s, Z, C]$.*

Theorem 4 (MoE oracle risk decomposition). *Let $g^*(Z) = \mathbb{P}(C = \text{crisis} | Z)$. Then for squared loss,*

$$\mathcal{R}(\hat{\varepsilon}_\theta) - \mathcal{R}(\hat{\varepsilon}^*) \leq c_1 \mathbb{E}[(g(Z) - g^*(Z))^2] + c_2 \sum_C \text{ApproxErr}_C,$$

where $\hat{\varepsilon}^* = (1 - g^*)\varepsilon_{\text{base}}^* + g^*\varepsilon_{\text{crisis}}^*$, and ApproxErr_C is the approximation error of each expert class.

Sketch. Expand the regression risk via law of total expectation and project onto the MoE span. The first term arises from gating misclassification; the second from function-class limits. \square

Corollary 1 (Crisis improvement under informative gating). *If g is monotone in the HMM crisis posterior (as in §3.6) and the crisis expert reduces tail MSE, then MoE strictly improves tail-region risk whenever $\mathbb{E}[(g - g^*)^2]$ is below a regime-dependent threshold.*

A.8 Stability of Gated Denoising and DDPM Sampling

Assumption 3 (Lipschitz experts and gate). *Each expert is L_ε -Lipschitz in (x, s) and the gate $g(Z)$ is L_g -Lipschitz in its inputs.*

Proposition 3 (Lipschitz constant of the MoE drift). *The MoE denoiser inherits Lipschitz constant $L_{\text{MoE}} \leq (1 + \|g\|_\infty)L_\varepsilon + L_g \Delta_\varepsilon$, where $\Delta_\varepsilon = \sup \|\varepsilon_{\text{crisis}} - \varepsilon_{\text{base}}\|$. Hence the DDPM reverse SDE/ODE remains contractive whenever L_{MoE} satisfies the usual step-size criteria.*

Remark 3. *This implies stability of sampling trajectories when the gate smoothly tracks regime posteriors (our HMM-derived $g_t = \sigma(\text{MLP}(z_t))$).*

A.9 Decision-Relevant Regret Bound for the CVaR Allocator

Let w^* solve the true-distribution QP (4)–(6) and \hat{w} the QP using blended/shrunk $(\hat{\mu}_t, \hat{\Sigma}_t)$ and sample CVaR under $p_\theta(\cdot | z_t)$.

Assumption 4 (Modeling error budgets). *There exist $\delta_\mu, \delta_\Sigma, \delta_{\text{CVaR}} \geq 0$ such that $\|\hat{\mu}_t - \mu^*\|_2 \leq \delta_\mu$, $\|\hat{\Sigma}_t - \Sigma^*\|_{\text{op}} \leq \delta_\Sigma$, and the CVaR term differs from truth by at most δ_{CVaR} uniformly over feasible w .*

Theorem 5 (Regret bound). *Let Γ be the strong convexity modulus of the QP objective in w induced by $\hat{\Sigma}_t$. Then*

$$F(\hat{w}) - F(w^*) \leq \frac{1}{2\Gamma} \left(\lambda_\mu \delta_\mu + \kappa_\Sigma \delta_\Sigma + \delta_{\text{CVaR}} \right)^2,$$

for suitable $\lambda_\mu, \kappa_\Sigma$ depending on budget/box/turnover radii. Moreover, if L_{tail} is small, then δ_{CVaR} is small by Proposition in A.5.

Sketch. Apply standard stability of strongly convex programs under objective perturbations, bounding the mean/variance terms by norm inequalities and the CVaR gap via A.5. \square

A.10 Quantile-Threshold Asymptotics for $Q_q(\tilde{\ell})$

Let \hat{Q}_q be the empirical q -quantile of $\tilde{\ell}$ used in L_{tail} . Under standard regularity (continuous density $f_{\tilde{\ell}}$ at Q_q),

$$\sqrt{N} (\hat{Q}_q - Q_q) \Rightarrow \mathcal{N}(0, q(1-q)/f_{\tilde{\ell}}(Q_q)^2).$$

Thus the randomness introduced by thresholding is $O_{\mathbb{P}}(N^{-1/2})$ and absorbed by the ESS of A.6 for moderate (q, η) .

Remark 4. *In practice, we use a running estimate of Q_q with exponential smoothing, which further stabilizes the gate into the weighted region while keeping the training unbiased on average.*

A.11 Tail-Weighted Diffusion as a Spectral Risk Upper-Bound

Recall L_{tail} in (7). Define a spectral weight $\phi(u) = 1 + \eta \mathbf{1}\{u \leq q\}$ on $u \in [0, 1]$, normalized by $\bar{\phi} = \int_0^1 \phi(u) du = 1 + \eta q$, and its probability measure $d\Phi(u) = \phi(u) du / \bar{\phi}$. Let $\mathcal{R}_\Phi(L)$ be the spectral risk of a loss L under Φ .

Assumption 5 (Tail-Lipschitz Decoder on tail set). *There exists $L_{\text{dec}} > 0$ s.t. on $\{\tilde{\ell} \leq Q_q(\tilde{\ell})\}$ we have $\|r - \hat{r}\| \leq L_{\text{dec}} \|\varepsilon - \varepsilon_\theta\|$.*

Theorem 6 (Spectral CVaR control by L_{tail}). *For any feasible w ,*

$$\left| \text{CVaR}_\alpha(-w^\top r) - \text{CVaR}_\alpha(-w^\top \hat{r}) \right| \leq \frac{L_{\text{dec}} \|w\|_2}{1 - \alpha} \sqrt{\bar{\phi} \mathbb{E}[\phi(U) \|\varepsilon - \varepsilon_\theta\|_2^2]},$$

where U is the PIT of $\tilde{\ell}$. Hence minimizing L_{tail} reduces a spectral upper-bound on the decision-relevant CVaR generalization gap.

Sketch. Express CVaR via Rockafellar–Uryasev’s tail average. Cauchy–Schwarz with tail reweighting ϕ yields the inequality; the decoder Lipschitz links denoising and return errors. \square

Remark 5. *Because allocation solves the convex CVaR epigraph QP in (4)–(6), decreasing this gap directly lowers the allocator’s risk mis-specification at decision time.*

A.12 Finite-Sample Efficiency of Tail Reweighting

Let $w_i = 1 + \eta \mathbf{1}\{\tilde{\ell}_i \leq Q_q(\tilde{\ell})\}$ and normalized $\bar{w}_i = w_i / \mathbb{E}[w_i]$.

Proposition 4 (Effective sample size). $\text{ESS} = N \frac{(1+\eta q)^2}{(1-q)+q(1+\eta)^2} = N \frac{1+2\eta q+\eta^2 q^2}{1+2\eta q+\eta^2 q}$.

Remark 6. *Moderate (q, η) (e.g., $q \in [0.05, 0.10]$, $\eta \in [1, 3]$) retains high ESS while emphasizing the adverse set that drives CVaR_α .*

A.13 Regime-MoE: Oracle Inequality, Consistency, and Stability

Let $\hat{\varepsilon}_\theta = (1 - g)\varepsilon_{\theta, \text{base}} + g\varepsilon_{\theta, \text{crisis}}$ with $g = g(Z) \in [0, 1]$.

Assumption 6 (Bayes experts + margin). *For $C \in \{\text{base}, \text{crisis}\}$, the Bayes denoiser ε_C^* lies in the closure of the expert class and there exists a margin $\gamma_m > 0$ such that $\mathbb{P}(|g^*(Z) - 1/2| \leq \gamma_m) \leq \kappa_m$ for some $\kappa_m < 1$.*

Theorem 7 (Oracle excess risk for MoE). *For squared loss,*

$$\mathcal{R}(\hat{\varepsilon}_\theta) - \mathcal{R}(\hat{\varepsilon}^*) \leq c_1 \mathbb{E}[(g - g^*)^2] + c_2 \sum_{C \in \{\text{base, crisis}\}} \text{ApproxErr}_C + c_3 \kappa_m,$$

where $\hat{\varepsilon}^* = (1 - g^*)\varepsilon_{\text{base}}^* + g^*\varepsilon_{\text{crisis}}^*$.

Proposition 5 (Gate consistency). *If g is trained with a calibrated surrogate (e.g., logistic) on HMM posteriors and the feature class has finite Rademacher complexity \mathfrak{R}_n , then $\mathbb{E}[(g - g^*)^2] = O(\mathfrak{R}_n) + o_n(1)$.*

Proposition 6 (Lipschitz MoE drift). *If experts are L_ε -Lipschitz in (x, s) and g is L_g -Lipschitz in Z , then the MoE drift is $L_{\text{MoE}} \leq (1 + \|g\|_\infty)L_\varepsilon + L_g \Delta_\varepsilon$, $\Delta_\varepsilon = \sup \|\varepsilon_{\text{crisis}} - \varepsilon_{\text{base}}\|$, ensuring stable DDPM steps.*

A.14 Allocation Mapping: Strong Convexity, Lipschitzness, and Regret

Let $\hat{w}(\hat{\mu}, \hat{\Sigma})$ solve the CVaR-QP (4)–(6) and assume $\hat{\Sigma} \succeq \lambda_{\min} I$.

Theorem 8 (Lipschitz solution map). *There exist constants (c_μ, c_Σ) such that for feasible perturbations $(\delta\mu, \delta\Sigma)$ with fixed constraints,*

$$\|\hat{w}(\hat{\mu} + \delta\mu, \hat{\Sigma} + \delta\Sigma) - \hat{w}(\hat{\mu}, \hat{\Sigma})\|_2 \leq \frac{c_\mu \|\delta\mu\|_2 + c_\Sigma \|\delta\Sigma\|_{\text{op}}}{\lambda_{\min}}.$$

Corollary 2 (Decision regret under moment & CVaR errors). *Let δ_{CVaR} bound the CVaR term perturbation uniformly over feasible w . If the objective is Γ -strongly convex in w , then*

$$F(\hat{w}) - F(w^*) \leq \frac{1}{2\Gamma} \left(\lambda_\mu \|\delta\mu\|_2 + \kappa_\Sigma \|\delta\Sigma\|_{\text{op}} + \delta_{\text{CVaR}} \right)^2.$$

Remark 7. By A.11, δ_{CVaR} shrinks with L_{tail} ; thus tail-weighted training tightens the end-to-end decision regret.

A.15 Distribution Shift View: CVaR Sensitivity under Wasserstein- W_1

Let losses be K -Lipschitz in r . For distributions P, Q with $W_1(P, Q) \leq \rho$,

Proposition 7 (CVaR Lipschitz continuity). $|\text{CVaR}_\alpha^P(L) - \text{CVaR}_\alpha^Q(L)| \leq \frac{K}{1-\alpha} \rho$.

Sketch. Use the tail-average representation of CVaR and Kantorovich–Rubinstein duality, noting the $1/(1-\alpha)$ amplification of tail averages. \square

Remark 8 (Interpretation). *Tail-aware generation (small L_{tail}) + bounded shift ρ jointly ensure limited CVaR drift, explaining empirical robustness under modest market shifts.*

A.16 Convex Pathwise Drawdown-CVaR Surrogate

For a horizon $\{t+1, \dots, t+H\}$ with scenarios $r_{t+1:t+H}^{(i)}$, introduce auxiliary peaks $p_h^{(i)}$ and drawdowns $d_h^{(i)}$:

$$p_h^{(i)} \geq p_{t-1}^{(i)} + w^\top r_{t+h}^{(i)}, \quad d_h^{(i)} \geq p_h^{(i)} - (p_t^{(i)} + \sum_{u=1}^h w^\top r_{t+u}^{(i)}), \quad \text{MDD}^{(i)} \geq d_h^{(i)}.$$

Then the convex surrogate program

$$\min_{w, \zeta, \{\text{MDD}^{(i)}\}, \dots} \zeta + \frac{1}{(1-\alpha)N} \sum_i (\text{MDD}^{(i)} - \zeta)_+ + \text{MV terms}$$

with budget/box/turnover constraints yields a CVaR-over-drawdown relaxation that stays QP-like after linearization, enabling direct drawdown control in multi-step allocation.

A.17 Envelope for Decision-Aware Training

Consider $V(\theta; z_t) = \min_{x \in X} F(x; \theta, z_t)$ where $x = (w, \zeta, \{u_i\}, s^+, s^-)$ and X fixes budget/box/turnover constraints (θ -independent). Then

Theorem 9 (Constraint-Independent Envelope). *If $F(\cdot; \theta, z_t)$ is continuously differentiable in θ and X does not depend on θ , then at any optimum $x^*(\theta; z_t)$,*

$$\nabla_\theta V(\theta; z_t) = \partial_\theta F(x^*(\theta; z_t); \theta, z_t).$$

Sketch. Direct envelope theorem: no constraint Jacobians in θ ; dual terms vanish from the gradient. \square

Corollary 3 (Smooth hinge surrogate for CVaR). *Replacing $(x)_+$ by a smooth $(1/\beta) \log(1 + e^{\beta x})$ yields $\nabla_\theta \mathbb{E}[V(\theta; z_t)] = \mathbb{E}[\partial_\theta F(x^*; \theta, z_t)]$, facilitating end-to-end training with a single QP solve per step.*

A.18 CVaR Estimation with Tail Reweighting

Let $\widehat{\text{CVaR}}_\alpha$ be the empirical epigraph estimator using N scenarios.

Assumption 7 (Tail regularity). *The loss distribution has continuous density near VaR_α and finite second moment on the lower tail.*

Theorem 10 (Rate with tail emphasis). *For weights $w_i = 1 + \eta \mathbf{1}\{\tilde{\ell}_i \leq Q_q(\tilde{\ell})\}$ normalized to \bar{w}_i ,*

$$|\widehat{\text{CVaR}}_\alpha - \text{CVaR}_\alpha| = O_{\mathbb{P}}\left(\sqrt{\frac{1}{\text{ESS}(q, \eta)}}\right),$$

with $\text{ESS}(q, \eta)$ from App. A.12. Moderate (q, η) balances bias/variance: higher tail mass can reduce variance of the tail average while keeping ESS large.

A.19 Gate Monotonicity \Rightarrow Tail-Region Risk Drop

Let $g^*(Z) = \mathbb{P}(C = \text{crisis} \mid Z)$ and suppose the crisis expert dominates on the tail region: $\mathbb{E}[\|\varepsilon - \varepsilon_{\text{crisis}}^*\|^2 \mid \tilde{\ell} \leq Q_q(\tilde{\ell})] \leq \mathbb{E}[\|\varepsilon - \varepsilon_{\text{base}}^*\|^2 \mid \tilde{\ell} \leq Q_q(\tilde{\ell})]$.

Proposition 8 (Tail-risk improvement under monotone gate). *If $g(Z)$ is non-decreasing in the HMM crisis posterior (Sec. 3.6), then for sufficiently small $\mathbb{E}[(g - g^*)^2]$, the MoE denoiser strictly reduces tail-region MSE versus either single expert.*

Sketch. Risk decomposition from the MoE oracle inequality (App. A.13) and the dominance assumption on the tail set. \square

A.20 End-to-End Decision Gap under Distribution Shift

Let P (train) and Q (test) satisfy $W_1(P, Q) \leq \rho$ for scenario distributions. Assume per-scenario loss $L(w, r)$ is K -Lipschitz in r for feasible w .

Theorem 11 (Shift-aware decision bound). *Let \hat{w} be the optimizer under P_θ and w_Q^* under Q . Then for the CVaR objective,*

$$F_Q(\hat{w}) - F_Q(w_Q^*) \leq \underbrace{c_1 L_{\text{tail}}^{1/2}}_{\text{train gen. gap}} + \underbrace{c_2 \rho/(1 - \alpha)}_{\text{shift gap}} + \underbrace{c_3 \|\hat{\mu} - \mu_Q\|_2 + c_4 \|\hat{\Sigma} - \Sigma_Q\|_{\text{op}}}_{\text{moment error}},$$

for constants (c_i) depending on feasible-set radii and strong convexity.

Sketch. Combine App. A.11 (spectral control), App. A.15 (CVaR W_1 continuity), and App. A.14 (allocator Lipschitz). \square